

Article

Fabrication of Transparent Mg(OH)₂ Thin Films by Drop-Dry Deposition

Tong Li  and Masaya Ichimura * 

Department of Electrical and Mechanical Engineering, Nagoya Institute of Technology, Gokiso, Showa, Nagoya 466-8555, Japan; 31413210@stn.nitech.ac.jp

* Correspondence: ichimura.masaya@nitech.ac.jp

Abstract: Magnesium hydroxide (Mg(OH)₂) thin films were deposited by the drop-dry deposition (DDD) method using an aqueous solution containing Mg(NO₃)₂ and NaOH. DDD was performed by dropping the solution on a substrate, heating-drying, and rinsing in water. Effects of different deposition conditions on the surface morphology and optical properties of Mg(OH)₂ thin films were researched. Films with a thickness of 1–2 μm were successfully deposited, and the Raman peaks of Mg(OH)₂ were observed for them. Their transmittance in the visible range was 95% or more, and the bandgap was about 5.8 eV. It was found that the thin films have resistivity of the order of 10⁵ Ωcm. Thus, the transparent and semiconducting Mg(OH)₂ thin films were successfully prepared by DDD.

Keywords: Mg(OH)₂; drop-dry deposition; transparent conductive thin film



Citation: Li, T.; Ichimura, M. Fabrication of Transparent Mg(OH)₂ Thin Films by Drop-Dry Deposition. *Materials* **2021**, *14*, 724. <https://doi.org/10.3390/ma14040724>

Academic Editor: Yun-Hyuk Choi
Received: 9 December 2020
Accepted: 1 February 2021
Published: 4 February 2021

Publisher's Note: MDPI stays neutral with regard to jurisdictional claims in published maps and institutional affiliations.



Copyright: © 2021 by the authors. Licensee MDPI, Basel, Switzerland. This article is an open access article distributed under the terms and conditions of the Creative Commons Attribution (CC BY) license (<https://creativecommons.org/licenses/by/4.0/>).

1. Introduction

In recent years, transparent conductive materials (TCMs) have been widely used as electrode materials for transparent electronics devices such as liquid crystal displays and touch panels, and also for thin film solar cells. Use of liquid crystal displays is rapidly spreading, and the demand for economical solar cells is increasing because of the climate change crisis. Thus, there is an increasing need for transparent electrodes. In addition, TCMs have begun to be used as semiconductors in devices such as thin film transistors (TFTs) [1–3]. Many oxides are transparent because they have a large bandgap, and transparent conductive oxides (TCOs) have been used for transparent electrodes. Among TCOs, indium tin oxide (ITO) has a low resistivity and a high transmittance and therefore is widely used at present. However, its constituent element indium is a rare metal, not abundant in the Earth's crust. Thus, there is a need for a material that can replace ITO, considering the possibility of resource depletion in the future. On the other hand, the most promising TCM for transparent TFTs is InGaZnO (IGZO) [4], but extensive research has also been carried out to develop TFT based on other materials such as ZnO [5] and SnO_x [6].

This study focused on magnesium hydroxide (Mg(OH)₂). Mg(OH)₂ has a bandgap of about 5.7 eV [7], is transparent to visible light, and has been generally used in the chemistry field as an antacid or flame retardant. The constituent element Mg is an abundant substance with the eighth largest Clarke number. Impurity doping in Mg(OH)₂ was investigated by first-principles calculation, and it was predicted that Mg(OH)₂ can have both n and p-type conductivity by proper impurity doping [8]. Several research groups actually fabricated solar cells with a Mg(OH)₂ layer inserted to enhance output voltage [9–11]. In addition, by reacting a carbon-doped Mg film with moisture, conductive carbon-doped Mg(OH)₂ with resistivity of the order of 10^{−2} or 10^{−3} Ωcm was prepared [12–15]. Thus, although Mg(OH)₂ has been traditionally regarded as an insulator, it can also be used as a semiconductor or conductor in electronics applications.

Many fabrication methods of Mg(OH)₂ have been reported, including the hydrothermal synthesis method [16], chemical precipitation method [17–23], sol-gel technique [24],

microwave-assisted synthesis [25], surfactant-mediated growth method [26], electrochemical deposition (ECD) method [27,28], etc. It was reported that Cu-doped $\text{Mg}(\text{OH})_2$ fabricated by ECD is semiconducting [29].

In this paper, we report the fabrication of $\text{Mg}(\text{OH})_2$ films by a simple technique: drop-dry deposition (DDD). DDD is a method of depositing a thin film by dropping and drying a solution on the substrate as shown in Figure 1. It uses a heating plate only and does not need other apparatuses, e.g., vacuum chamber, electric power supply, or light source. Thus, the apparatus required by DDD is simple and easy to use, and therefore DDD is advantageous for deposition of a thin film over a large area at a low cost. As shown below, the deposited $\text{Mg}(\text{OH})_2$ films are highly transparent and semiconducting.

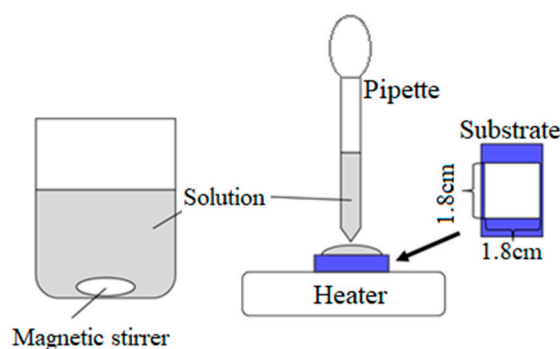


Figure 1. Apparatus of the drop-dry deposition method.

2. Experiments

For the $\text{Mg}(\text{OH})_2$ preparation, $\text{Mg}(\text{NO}_3)_2$ and NaOH were dissolved in pure water. After mixing, $\text{Mg}(\text{OH})_2$ was spontaneously synthesized by the reaction:



Without stirring, $\text{Mg}(\text{OH})_2$ particles are physically entangled to form aggregates of a specific size. However, with stirring, the entanglement is loosened [30], and a uniform, slightly hazy solution was obtained.

The substrate was alkali-free glass. Several samples were also prepared on quartz substrates for optical characterization. Before the thin film deposition, the substrate was degreased and washed with acetone and pure water, and the deposition area was limited to $1.8 \times 1.8 \text{ cm}^2$ by masking. The deposition solution was dropped on the substrate using a pipette. Then, the substrate was heated at $60 \text{ }^\circ\text{C}$ using a heater plate until the water was evaporated completely. The time required for drying was about 10 min when 0.2 mL was dropped. Then, the substrate was rinsed with pure water and blown by a nitrogen gas. During the drying process, $\text{Mg}(\text{OH})_2$, which has low solubility in water, first precipitates and is deposited on the substrate. After that, other solutes, having higher solubility, precipitate on the film, and then they are washed away in the subsequent rinsing process. The steps of the solution dropping and drying were repeated several times to deposit the thin film.

The deposition was carried out under the following conditions:

- Number of drop-dry cycles: 5, 10 ($\text{Mg}(\text{NO}_3)_2$: 25 mM, NaOH : 50 mM).
- $\text{Mg}(\text{NO}_3)_2$ concentrations: 10, 20, 30, 40, 50 mM (NaOH : 50 mM, cycles: 5).
- NaOH concentrations: 25, 50, 100 mM ($\text{Mg}(\text{NO}_3)_2$: 25 mM, cycles: 5).

Film thickness and surface roughness were measured by an Accretch Surfcom-1400D profilometer. Optical transmittance measurement was performed using a Jasco V-570 UV/VIS/NIR spectrometer. Auger electron spectroscopy (AES) data and scanning electron microscope (SEM) images were obtained using a JEOL JAMP-9500F field emission microprobe (JEOL LTD., Akishima, Japan) at a probe voltage of 10 keV. Raman spectroscopy measurement was performed with excitation laser wavelength of 532 nm using a Jasco

NRS-3300 Raman spectroscope (JASCO Corporation, Tokyo, Japan). X-ray diffraction (XRD) experiments were performed with a SmartLab X-ray diffractometer (Rigaku) using a Cu K α radiation source. For the electrical characterization, indium inter-digit electrodes were fabricated by vacuum evaporation on the thin film prepared on the alkali-free glass substrate, and then current-voltage (I-V) measurement was performed.

3. Results and Discussion

3.1. Deposition Conditions

Thickness was measured for the thin films prepared under the various deposition conditions noted above. When the deposition cycle was repeated five times, the film thickness was about 2.0 μm . When the drop-dry (DD) cycle number exceeded seven, the film began to become hazy or porous. Then, the apparent thickness increased steeply, and the film became mechanically weak. When the cycle number was increased to 10, the average thickness increased to about 10 μm , with nonuniformity much enhanced. The thickness was more than 10 μm in some parts, but some parts of the film fell off the substrate. With increasing $\text{Mg}(\text{NO}_3)_2$ concentration (10–40 mM), the film thickness increased from 0.7 μm to 3.0 μm , and its nonuniformity became larger. At 50 mM, a part of the thin film was broken and fell off the substrate. With increasing NaOH concentration (10–100 mM), the film thickness increased from 0.8 μm to 2.2 μm , and the uniformity did not change significantly.

Figure 2 shows the optical transmittance of the thin films prepared under different deposition conditions. The data plotted in Figure 2 were obtained by dividing the transmittance of the sample by the reference data taken for the glass substrate without any deposit on it. As shown in Figure 2a, the sample deposited with 5 cycles showed transmittance of 95% or more in the visible region, but the sample deposited with 10 cycles had lower transmittance (65–90%) in the visible region: The 10-cycle sample was hazy. Figure 2b shows the influence of $\text{Mg}(\text{NO}_3)_2$ concentration. For $\text{Mg}(\text{NO}_3)_2$ concentrations ≤ 30 mM, the samples showed high transmittance (>90%) in the visible region. However, when the concentration of $\text{Mg}(\text{NO}_3)_2$ was 40 mM or more, the transmittance was significantly decreased, 65–95% in the visible region. Although the transmittance tended to decrease with increasing $\text{Mg}(\text{NO}_3)_2$ concentration, the transmittance was higher for 30 mM than for 20 mM. This could be because of nonuniformity in surface roughness: the data for 20 mM are considered to be affected by local surface roughness. Thus, the reproducibility is not good enough to discuss a difference of a few percentage points in transmittance. Figure 2c shows the effects of NaOH concentration. The samples deposited with NaOH concentrations of 25, 50, and 100 mM showed transmittance of 95% or more in the visible region, and thus the effects of NaOH concentration are not significant. The transmittance of some samples appeared to exceed 100% because of lower reflectance of $\text{Mg}(\text{OH})_2$ than glass. As noted above, the glass substrate was used as a reference. Since $\text{Mg}(\text{OH})_2$ has a larger bandgap, the refractive index of $\text{Mg}(\text{OH})_2$ is expected to be lower than that of glass. Thus, for the glass substrate with $\text{Mg}(\text{OH})_2$ on it, the reflectance is lower and the transmitted light power can be higher than for that of the bare glass substrate. Then, the apparent transmittance value exceeds 100%. It should be noted that the transmittance did not exceed 100% when a quartz substrate was used, as shown below. This is because quartz has a larger bandgap and lower refractive index than $\text{Mg}(\text{OH})_2$.

Considering both the thickness and transmission results, we can conclude that when the thickness exceeds 3 μm , the roughness and nonuniformity become so large that the transmittance in the visible range is significantly low. In the following characterization, we adopted the deposition conditions: 25 mM $\text{Mg}(\text{NO}_3)_2$, 50 mM NaOH, and 5 deposition cycles. Under this condition, the film thickness was about 2 μm , and the transmittance was 95% or more in the visible range. The thickness profile measurement results are shown in Figure 3. We repeated deposition under these conditions, and the film thickness and transmittance were reproduced with deviations of about 5%.

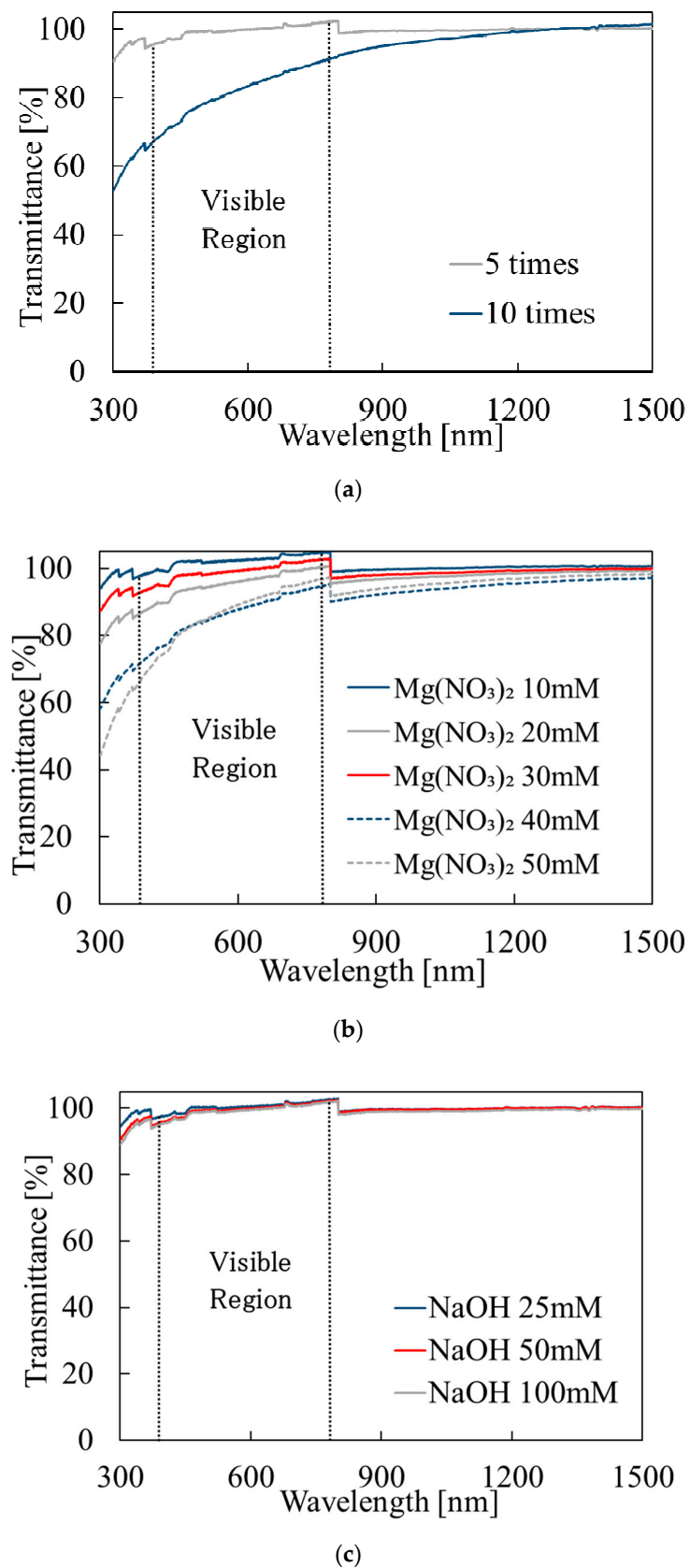


Figure 2. Optical transmittance under each deposition condition: (a) change in the number of depositions; (b) change in $\text{Mg}(\text{NO}_3)_2$ concentration; (c) change in NaOH concentration. (The steps near 800 nm were caused by sensor changes in the spectrophotometer, and we failed to calibrate the signal level.)

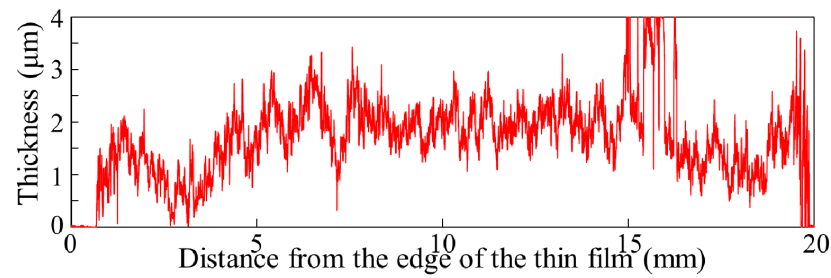


Figure 3. Surface roughness measurement results of the $\text{Mg}(\text{OH})_2$ film.

3.2. Characterization of the Films

To evaluate the bandgap, we deposited the film on a quartz substrate, which does not absorb UV light (>200 nm). The transmittance measurement results and the bandgap calculation results are shown in Figures 4 and 5, respectively. To observe absorption due to the film, the transmittance of the quartz substrate was measured as the reference. According to the first-principles calculation, the band structure of $\text{Mg}(\text{OH})_2$ is direct [31], and thus the band gap can be evaluated by plotting $(\alpha h\nu)^2$ vs. $h\nu$, where α is the absorption coefficient and $h\nu$ is the photon energy. The bandgap for the as-deposited film was found to be around 5.8 eV, which closely matches the reported values [7].

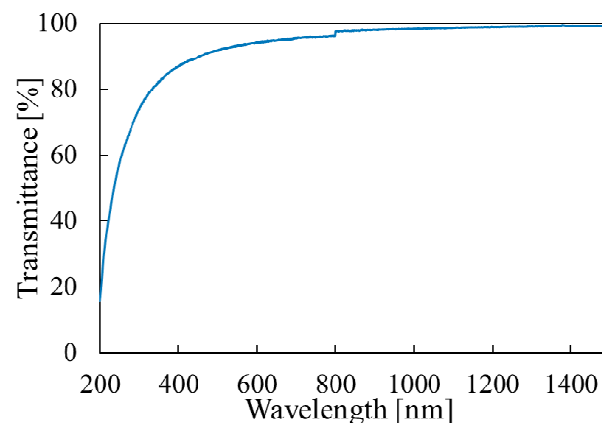


Figure 4. Optical transmittance measurement results of the $\text{Mg}(\text{OH})_2$ film.

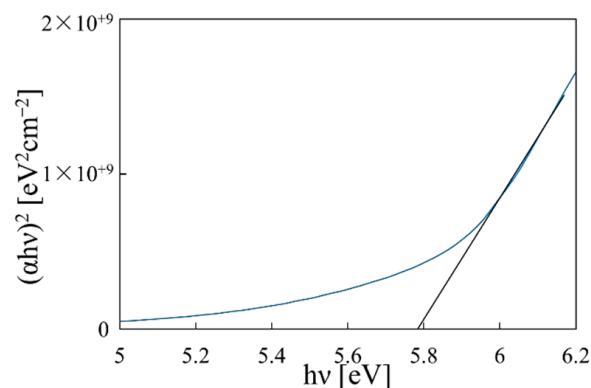


Figure 5. Bandgap evaluation of the $\text{Mg}(\text{OH})_2$ film.

The SEM image of the thin film is shown in Figure 6. Grain images were not observed on the surfaces. In the AES measurement, only the signals of Mg and O were detected, as shown in Figure 7. Thus, by the rinsing process, the contents of the other elements contained in the deposition solution (Na, N) were reduced to below the detection limit of AES (about 1%).

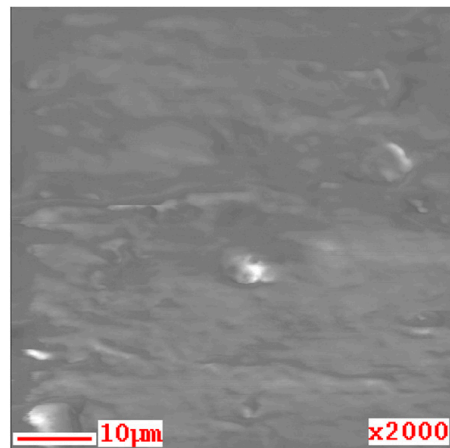


Figure 6. SEM image of the Mg(OH)₂ film.

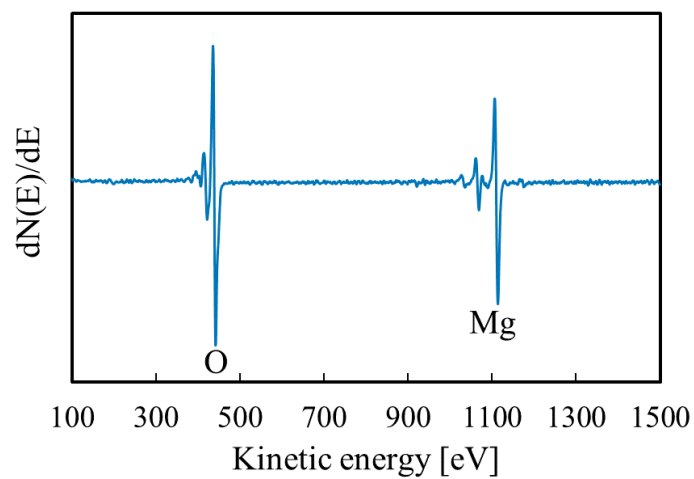


Figure 7. AES spectra of the Mg(OH)₂ film.

The Raman measurement results are shown in Figure 8. The peaks of Mg(OH)₂ and alkali-free glass (substrate) were observed for the thin film [32]. To clarify the structural properties, XRD measurements were also carried out. However, we did not observe any peaks, as shown in Figure 9. Therefore, we think that the films are amorphous.

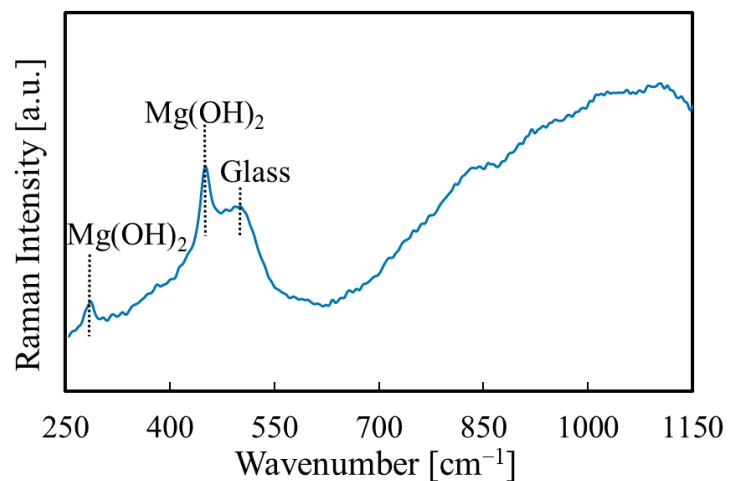


Figure 8. Raman spectrum of the Mg(OH)₂ film.

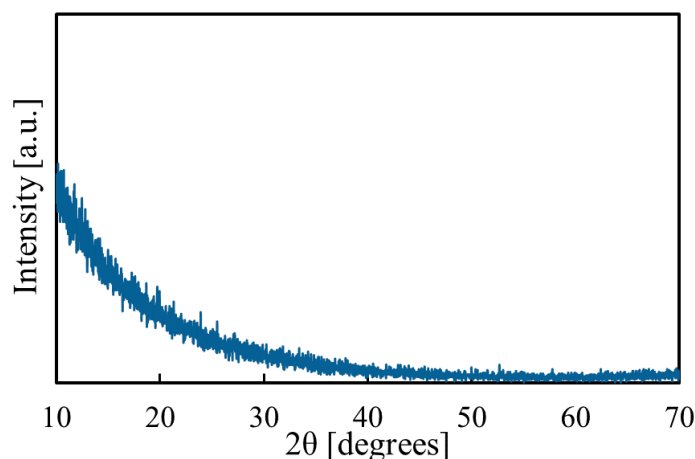


Figure 9. XRD of the $\text{Mg}(\text{OH})_2$ film.

In the I-V measurement, ohmic behaviors were observed. It was confirmed that alkali-free glass substrates are insulating, and thus the observed current was due to conduction in the film parallel to the surface. Six pairs of electrodes were formed on a sample. The resistivity values calculated from the I-V data were scattered in a range from 4.4 to $8.5 \times 10^5 \Omega\text{cm}$.

3.3. Discussion

The I-V results indicate that the films are not insulating but semiconducting. The origin of the conductivity of the $\text{Mg}(\text{OH})_2$ films is not understood. According to the first-principles calculation, both native defects and impurities can donate carriers in $\text{Mg}(\text{OH})_2$ [8]. Possible impurities are Na^+ from NaOH and NO_3^- from $\text{Mg}(\text{NO}_3)_2$. Although Na and N were not found in the AES measurement, a trace amount of them could be contained in the films and affect the conductivity. In the future, we will attempt intentional impurity doping to control the resistivity. If n- and p-type conductivity of $\text{Mg}(\text{OH})_2$ is controlled through doping, then $\text{Mg}(\text{OH})_2$ can be used as a transparent semiconductor to fabricate devices such as diodes and transistors.

Although deposition of dispersions and subsequent drying is a common process for preparing a film, the drying process has not been utilized for fabricating flat, transparent, thin films in electronics. We attempted for the first time to fabricate transparent semiconductor films by DDD in this work. DDD would be advantageous for transparent electronics because films can be deposited at low temperatures using a heater plate only. To deposit a film in a large area by DDD, care must be taken to evenly spread the solution over the entire deposition surface. The solution should be dropped not at a single point but at multiple points.

4. Conclusions

In this study, $\text{Mg}(\text{OH})_2$ thin films were prepared by drop-dry deposition using an aqueous solution containing $\text{Mg}(\text{NO}_3)_2$ and NaOH, and their elemental composition and optical and electrical properties were evaluated. Optical transmittance in the visible range was 95% or more for the samples with a thickness of about 2 μm . The Raman peaks of $\text{Mg}(\text{OH})_2$ were observed for the as-deposited film. The bandgap was about 5.8 eV, and the resistivity was of the order of $10^5 \Omega\text{cm}$.

Author Contributions: Conceptualization, M.I.; resources, M.I.; supervision, M.I.; investigation, T.L.; writing—original draft preparation, T.L.; writing—review and editing, M.I. All authors have read and agreed to the published version of the manuscript.

Funding: This research received no external funding.

Institutional Review Board Statement: Not applicable.

Informed Consent Statement: Not applicable.

Data Availability Statement: The data is contained within the article.

Conflicts of Interest: The authors declare no conflict of interest.

References

1. Hosono, H. Recent progress in transparent oxide semiconductors: Materials and device application. *Thin Solid Films* **2007**, *515*, 6000–6014. [[CrossRef](#)]
2. Fortunato, E.; Barquinha, P.; Martins, R. Oxide semiconductor thin-film transistors: A review of recent advances. *Adv. Mater.* **2012**, *24*, 2945–2986. [[CrossRef](#)] [[PubMed](#)]
3. Tiwari, N.; Nirmal, A.; Kulkarni, M.R.; John, R.A.; Mathews, N. Enabling high performance n-type metal oxide semiconductors at low temperatures for thin film transistors. *Inorg. Chem. Front.* **2020**, *7*, 1822–1844. [[CrossRef](#)]
4. Kamiya, T.; Nomura, K.; Hosono, H. Present status of amorphous In–Ga–Zn–O thin-film transistors. *Sci. Technol. Adv. Mater.* **2010**, *11*, 044305. [[CrossRef](#)]
5. Nishii, J.; Hossain, F.M.; Takagi, S.; Aita, T.; Saikusa, K.; Ohmaki, Y.; Ohkubo, I.; Kishimoto, S.; Ohtomo, A.; Fukumura, T.; et al. High mobility thin film transistors with transparent ZnO channels. *Jpn. J. Appl. Phys.* **2003**, *42*, L347–L349. [[CrossRef](#)]
6. Nomura, K.; Kamiya, T.; Hosono, H. Ambipolar oxide thin-film transistor. *Adv. Mater.* **2011**, *23*, 3431–3434. [[CrossRef](#)]
7. Kumari, L.; Li, W.Z.; Vannoy, C.H.; Leblanc, R.M.; Wang, D.Z. Synthesis, characterization and optical properties of Mg(OH)₂ micro-/nanosstructure and its conversion to MgO. *Ceram. Int.* **2009**, *35*, 3355–3364. [[CrossRef](#)]
8. Ichimura, M. Impurity doping in Mg(OH)₂ for n-type and p-type conductivity control. *Materials* **2020**, *13*, 2972. [[CrossRef](#)]
9. Miyazaki, H.; Mikami, R.; Yamada, A.; Konagai, M. Chemical-bath-deposited ZnO and Mg(OH)₂ buffer layer for Cu(InGa)Se₂ solar cells. *Jpn. J. Appl. Phys.* **2006**, *45*, 2618–2620. [[CrossRef](#)]
10. Yum, J.H.; Nakade, S.; Kim, D.Y.; Yanagida, S. Improved performance in dye-sensitized solar cells employing TiO₂ photoelectrodes coated with metal hydroxides. *J. Phys. Chem. B* **2006**, *110*, 3215–3219. [[CrossRef](#)]
11. Nirmal Peiris, T.A.; Senthilarasu, S.; Upul Wijayantha, K.G. Enhanced performance of flexible dye-sensitized solar cells: Electrodeposition of Mg(OH)₂ on a nanocrystalline TiO₂ electrode. *J. Phys. Chem. C* **2012**, *116*, 1211–1218. [[CrossRef](#)]
12. Honjo, T.; Chiba, M.; Kuji, T. Novel rare-elements free transparent conductor of Mg(OH)₂-C compounds. *e-J. Surf. Sci. Nanotechnol.* **2009**, *7*, 791–794. [[CrossRef](#)]
13. Murakami, T.; Honjo, T.; Kuji, T. DOS calculation analysis of new transparent conductor Mg(OH)₂-C. *Mater. Trans.* **2011**, *52*, 1689–1692. [[CrossRef](#)]
14. Guo, S.; Yang, L.; Dai, B.; Geng, F.; Yang, Z.; Wang, P.; Gao, G.; Lei, P.; Han, J.; Ralchenko, V.; et al. Wide-range infrared transparency of hydrated magnesium-carbon films with high mobility for enhanced conductivity. *Surf. Coat. Technol.* **2019**, *365*, 70–75. [[CrossRef](#)]
15. Guo, S.; Yang, L.; Dai, B.; Geng, F.; Yang, Z.; Lei, P.; Wang, P.; Gao, G.; Han, J.; Ralchenko, V.; et al. Effect of annealing treatment on transparent and conductive hydrated magnesium-carbon films. *J. Alloys Compd.* **2019**, *778*, 83–89. [[CrossRef](#)]
16. Zhu, Y.; Zhao, Q.; Zhang, Y.H.; Wu, G. Hydrothermal synthesis of protective coating on magnesium alloy using de-ionized water. *Surf. Coat. Technol.* **2012**, *206*, 2961–2966. [[CrossRef](#)]
17. Wang, P.; Li, C.; Gong, H.; Wang, H.; Liu, J. Morphology control and growth mechanism of magnesium hydroxide nanoparticles via a simple wet precipitation method. *Ceram. Int.* **2011**, *37*, 3365–3370. [[CrossRef](#)]
18. Yousefi, S.; Ghasemi, B.; Tajally, M.; Asghari, A. Optical properties of MgO and Mg(OH)₂ nanostructures synthesized by a chemical precipitation method using impure brine. *J. Alloys Compd.* **2017**, *711*, 521–529. [[CrossRef](#)]
19. Hsu, J.P.; Nacu, A. Preparation of submicron-sized Mg(OH)₂ particles through precipitation. *Colloid Surf. A Physicochem. Eng. Asp.* **2005**, *262*, 220–231. [[CrossRef](#)]
20. Suárez-Campos, G.; Cabrera-German, D.; García-Valenzuela, J.A.; Cota-Leal, M.; Fuentes-Ríos, J.L.; Martínez-Gil, M.; Hu, H.; Sotelo-Lerma, M. Controlled synthesis of Mg(OH)₂ thin films by chemical solution deposition and their thermal transformation to MgO thin films. *Ceram. Int.* **2019**, *45*, 10356–10363. [[CrossRef](#)]
21. Raza, S.M.; Ali, R.S.; Naeem, M.; Uddin, Z.; Qaseem, S.; Ali, I.S.; Shah, N.S. Tuning the bandgap in co-doped Mg(OH)₂ nanoparticles. *Int. J. Mod. Phys. B* **2019**, *33*, 1950182. [[CrossRef](#)]
22. Lu, L.; Hua, Q.; Tang, J.; Liu, Y.; Liu, L.; Baoming, W. Reactive crystallization kinetics of magnesium hydroxide in the Mg(NO₃)₂-NaOH system. *Cryst. Res. Technol.* **2018**, *53*, 1700310. [[CrossRef](#)]
23. Henrist, C.; Mathieu, J.P.; Vogels, C.; Rulmont, A.; Cloots, R. Morphological study of magnesium hydroxide nanoparticles precipitated in dilute aqueous solution. *J. Cryst. Growth* **2003**, *249*, 321–330. [[CrossRef](#)]
24. Baird, T.; Braterman, P.S.; Cochrane, H.D.; Spoons, G. Magnesium hydroxide precipitation as studied by gel growth methods. *J. Cryst. Growth* **1988**, *91*, 610–616. [[CrossRef](#)]
25. Al-Gaashani, R.; Radiman, S.; Al-Douri, Y.; Tabet, N. Investigation of the optical properties of Mg(OH)₂ and MgO nanostructures obtained by microwave-assisted methods. *J. Alloys Compd.* **2012**, *521*, 71–76. [[CrossRef](#)]
26. An, D.; Ding, X.; Wang, Z.; Liu, Y. Synthesis of ordered arrays of magnesium hydroxide nanoparticles via a simple method. *Colloid Surf. A Physicochem. Eng. Asp.* **2010**, *356*, 28–31. [[CrossRef](#)]
27. Keikhaei, M.; Ichimura, M. Fabrication of Mg(OH)₂ thin films by electrochemical deposition with Cu catalyst. *Thin Solid Films* **2019**, *681*, 41–46. [[CrossRef](#)]
28. Zou, G.; Chen, W.; Liu, R.; Xu, Z. Morphology-tunable synthesis and characterizations of Mg(OH)₂ films via a cathodic electrochemical process. *Mater. Chem. Phys.* **2008**, *107*, 85–90. [[CrossRef](#)]

-
29. Keikhaei, M.; Ichimura, M. N-type and p-type semiconducting Cu-doped Mg(OH)₂ thin films. *Semicond. Sci. Technol.* **2020**, *35*, 035020. [[CrossRef](#)]
 30. Hideki, T. Reactive crystallization of magnesium hydroxide. *Bull. Soc. Sea Water Sci. Jpn.* **1997**, *51*, 348–357.
 31. Pishtshev, A.; Karazhanov, S.Z.; Klopov, M. Materials properties of magnesium and calcium hydroxides from first-principles calculations. *Comput. Mater. Sci.* **2014**, *95*, 693–705. [[CrossRef](#)]
 32. Dawson, P.; Hadfield, C.D.; Wilkinson, G.R. The polarized infra-red and Raman spectra of Mg(OH)₂ and Ca(OH)₂. *J. Phys. Chem. Solids* **1973**, *34*, 1217–1225. [[CrossRef](#)]